Hindawi
Journal of Chemistry
Volume 2022, Article ID 1236621, 19 pages
https://doi.org/10.1155/2022/1236621

Research Article

Adsorption of Indigo Carmine onto Chemically Activated Carbons Derived from the Cameroonian Agricultural Waste *Garcinia cola* Nut Shells and Desorption Studies

Idris-Hermann Tiotsop Kuete,[1] **Raoul Donald Tchuifon Tchuifon**,[1,2] **Aurelien Bopda**,[1] **Christian Sadeu Ngakou**,[1] **George Ndifor-Angwafor Nche**,[1] **and Solomon Gabche Anagho**[1]

[1]*Materials and Process Engineering Team (MPET), Research Unit of Noxious Chemistry and Environmental Engineering (RUNOCHEE), Department of Chemistry, Faculty of Science, University of Dschang, P.O. Box 67, Dschang, Cameroon*
[2]*Laboratory of Energy Materials Modeling and Method, Department of Process Engineering, National Higher Polytechnic School of Douala, University of Douala, Douala, Cameroon*

Correspondence should be addressed to Solomon Gabche Anagho; sg_anagho@yahoo.com

Received 11 May 2022; Revised 25 June 2022; Accepted 5 July 2022; Published 31 August 2022

Academic Editor: Gonggang Liu

In the quest for a sustainable environment and clean water resources, the efficacy of activated carbons synthesized from *Garcinia cola* nut shells impregnated with KOH ($CBK_{1/1}$) and $ZnCl_2$ ($CBZ_{1/1}$) for the adsorption of indigo carmine (IC) dye was studied using the batch technique. The prepared activated carbons were characterized using iodine number, elemental analysis, scanning electron microscopy (SEM), FTIR spectroscopy, powder X-ray diffraction (XRD), TGA/DTA, Boehm titration, and pH at point of zero charge. The elemental analysis showed a high percentage of carbon in both activated carbons (ACs). FTIR and Boehm titration analysis indicated the presence of several functional groups on the surfaces of both ACs which could influence the adsorption of IC. The primary adsorption mechanisms involved electrostatic interaction, hydrogen bonds formation, and π–π interactions. Maximum adsorption capacity values obtained using the Fritz–Schlunder III three-parameter model were 19.019 $mg{\cdot}g^{-1}$ and 18.299 $mg{\cdot}g^{-1}$ for $CBK_{1/1}$ and $CBZ_{1/1}$, respectively. The Fritz–Schlunder model exponent m_{FS} of value less than 1 showed that the adsorption of IC by the ACs occurred on heterogeneous surfaces. Positive values of ΔQ obtained by the linear and nonlinear forms of the Temkin model indicate the exothermic character of the adsorption process.

1. Introduction

Nowadays, several industries discharge their colored effluents containing synthetic dyes into aquatic environments [1]. These dyes are considered as chief contaminants in water since they pose serious threats to human beings and aquatic organisms [2]. Wastewater is often discharged into rivers and lakes or infiltrates into aquifers, where it can affect the quality of freshwater supplies. Globally, over 80% of the wastewater sent into the environment without treatment causes negative consequences for the marine environment [3]. Water pollution by dyes is becoming a major environmental problem since colouring agents cause significant environmental damage to both human health and aquatic organisms. These dyes are highly toxic, carcinogenic, mutagenic, teratogenic, and stable during aerobic degradation [4]. The discharges of industrial wastewater containing very low concentrations of dyes reduce light penetration through the water surface, precluding photosynthesis of the aqueous flora.

Indigo carmine dye is used in the textile industry for dyeing clothes and in cosmetics, plastics, and paper mills, while in medicine, it is used as an aid to diagnosis [5]. Indigo

carmine is considered in the class of the highly toxic indigoid dyes. Its contact with the skin can cause irritation, while with the eye, it can cause both irritation and permanent injury to the cornea and conjunctiva [6].

Consumption of this dye at high concentration has also been shown to be fatal, as it is carcinogenic by nature and can cause reproductive, developmental, neurological, and acute toxicity [6]. It has also been reported to cause mild-to-severe hypertension and cardiovascular and respiratory effects [6]. According to the World Health Organization standards, the limit concentration of indigo carmine is $0.005\,mg{\cdot}L^{-1}$ [7]. Thus, indigo carmine is not only a noxious substance to aquatic life but also to us humans. Therefore, the elimination of this type of dye in wastewater or at the exit of industries becomes a major concern.

Several techniques have been discussed in the literature for the removal of dyes from water and wastewater. Among these techniques, adsorption is considered the most economically favorable among those available, such as membrane separation, oxidation, and irradiation, because of its high removal efficiency, low operation cost, and its ability to separate a wide range of contaminants from industrial effluents [8].

Amongst the adsorbents used in the adsorption processes, one of the most widespread for the removal of contaminants from water is activated carbon (AC) [9,10] which, due to its pore structure and various functional groups on its surface, provides exceptional adsorption capacity. Different activating carbons can be manufactured by exploiting a wide variety of carbonaceous precursors such as coal, petroleum, peat, wood, and agricultural wastes [11], resulting in the production of a variety of adsorbents with different characteristics and qualities.

The use of biomass waste for the preparation of porous activated carbon has increased considerably in recent years. Some of the residual biomasses used for the manufacture of activated carbons are coffee waste [9], tucumã seeds [10], Ayous sawdust and Cucurbitaceae peelings [12], rice and coffee husks [13], olives stones and cotton cake [14], *Vitellaria paradoxa* [15], and rice hull and tamarind (*T. indica*) seeds [16].

This work had a double interest: valorizing the residues coming from a Cameroonian biomass to prepare activated carbons using chemical treatment techniques and testing their performance in the water treatment. In this work, the residual biomass, *Garcinia cola* nut shells from Cameroon, was proposed as a raw material for the development of activated carbons by chemical activation using KOH and $ZnCl_2$, in order to recycle these wastes that are currently generated in large quantities and are of little use in Cameroon [17].

In this research, the feasibility of producing activated carbons suitable for the efficient removal of indigo carmine was demonstrated.

Specifically, this research was subdivided into three parts:

(i) Production of activated carbons from *Garcinia cola* nut shells by chemical activation with KOH and $ZnCl_2$

(ii) Application of the activated carbons as adsorbents for the removal of indigo carmine in aqueous solution and evaluation of their efficacy

(iii) Demonstration of the reusability of each adsorbent by studying desorption

2. Materials and Methods

2.1. Preparation of Activated Carbons. ACs were produced by the following procedure: first, 200 g of particles of dried *Garcinia cola* nut shell (CB) with diameters varying between 250 and 1000 μm was blended in a 1 : 1 weight ratio with the activating agent KOH or $ZnCl_2$. Each resulting paste was dried and placed in a porcelain crucible with lid and introduced into an electric furnace of mark ISUNU and heated from the ambient temperature up to 400°C, using a heating rate of $5^{\circ}C{\cdot}min^{-1}$ in absence of CO_2, H_2O, O_2, and N_2 gases. The temperature of the furnace was kept fixed at the maximum temperature of 400°C for 1 hour. It was then allowed to cool to room temperature, and the activated carbon obtained was washed with distilled water until the excess activating agent was removed. The samples were coded as $CBK_{1/1}$ and $CBZ_{1/1}$, respectively, according to KOH and $ZnCl_2$ used as the activating agent.

2.2. Characterization. Activated carbons were characterized to determine the surface functional groups by Fourier-transform infrared (FTIR) spectroscopy using a Nicolet iS5 FTIR Spectrometer. The physical and chemical characteristics of both activated carbons were found out by ASTM methods. Thermogravimetric analysis of both activated carbons was performed on STA 409 CD thermos-balance with a heating rate of $10^{\circ}C{\cdot}min^{-1}$ in a nitrogen flow and temperature range of 50–1500°C. Elemental analysis of both activated carbons was determined using CHNS elemental analyses from the HEKAtech CHNS Analyzer. Scanning electron images of the two activated carbons were obtained using a scanning electron microscope, furnished by sputter coater analysis. Crystalline structure of the activated carbons was analyzed by X-ray diffraction (XRD) analysis using a STOE Stadi-p X-ray powder diffractometer (STOE & Cie GmbH, Darmstadt, Germany). Figure 1 shows the preparation and characterization steps for the different activated carbons.

2.3. Adsorbate. Stock solution of indigo carmine at $500\,mg{\cdot}L^{-1}$ was prepared by dissolving a previously calculated mass of 123.75 mg of the latter in a 250 mL volumetric flask containing 100 mL of distilled water, homogenize until the pollutant is completely dissolved, and then make up to the mark and store in a dark place. The working indigo carmine solution was prepared by diluting the stock solution with distilled water. Figure 2 shows the 3D structure of indigo carmine.

2.4. Adsorption and Desorption Studies. Batch adsorption studies were carried out at room temperature by mechanical agitation at a constant speed of 200 rpm to deduce the

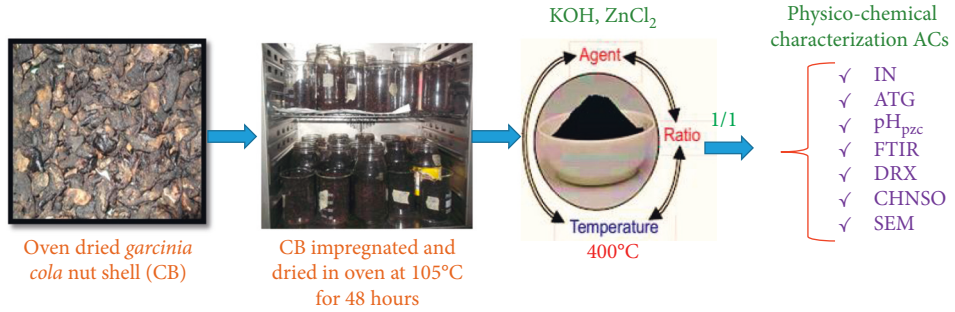

Figure 1: Preparation and characterization of activated carbons.

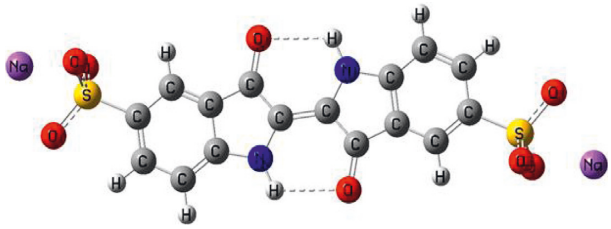

Figure 2: 3D structure of indigo carmine ($C_{16}H_8N_2Na_2O_8S_2$).

optimum pH, contact time, adsorbent mass, initial indigo carmine concentration, and the effect of ionic strength. For each run, 20 mL of indigo carmine dye solution of known initial concentration varying between 30 and 100 mg L^{-1} was treated with 100 mg each of the activated carbons, $CBK_{1/1}$ and $CBZ_{1/1}$, at optimum pH. The pH value of each solution was adjusted by addition of 0.1 M solution of HCl or NaOH. After agitation, the solution was filtered using the Whatman no.1 filter paper, and the filtrate was analyzed to obtain the residual concentration of indigo carmine using a UV/Vis spectrophotometer (Jenway, model 6715) at a wavelength (λ) of 610 nm. Similar measurements were carried out by varying the pH of the solution (2–8), contact time (5–120 min), adsorbent mass (50–400 mg), and ionic strength varying NaCl concentration (0.01–0.06 mol·L^{-1}). The amount of dye adsorbed (Q_e) and the percentage removal (%ads) of dye were calculated using the following expressions:

$$Q_e = \frac{(C_0 - C_e)}{m} \cdot V,$$
$$\%\text{ads} = \frac{(C_0 - C_e)}{C_0} \cdot 100, \quad (1)$$

where C_0 is the initial concentration of the dye, C_e is the concentration of the dye at the equilibrium time, V is the volume of the adsorbate solution, and m is the mass of the adsorbent.

For the desorption studies, 400 mg of each adsorbent was mixed in a flask with 100 mL of indigo carmine dye solution at an initial concentration of 50 mg·L^{-1}. Mixtures were stirred at a constant speed of 200 rpm for 80 min. After stirring, suspensions were filtered and filtrates were analyzed by measuring absorbance using a UV-Visible spectrophotometer. Indigo carmine loaded with each adsorbent was collected after filtration and was dried in an oven at 105°C, and 50 mg of each of these materials was contacted with 10 mL of desorption solutions of 4×10^{-2} mol·L^{-1} of NaOH or H_2SO_4 and 10 mL of H_2O. The mixtures were stirred at a constant speed of 200 rpm for 80 min. After stirring, suspensions were filtered and filtrates were analyzed by measuring absorbance using a UV-Visible spectrophotometer. Desorption percentages (%des) were calculated by the following equation [18, 19]:

$$\%_{des} = \frac{C_f - C_r}{C_f}.100, \quad (2)$$

where C_f (mg·L^{-1}) is the initial concentration of dyes loaded with each adsorbent and C_r (mg·L^{-1}) is the final concentration of dyes loaded with each adsorbent.

2.5. Equilibrium and Kinetic Studies. In this work, four two-parameter adsorption isotherm models (Langmuir, Freundlich, Temkin, and Halsey), one three-parameter model (Fritz–Schlunder III), and five kinetic models (pseudo-first order, pseudo-second order, Avrami kinetics, intraparticle diffusion, and Boyd) were tested. In the aim to study the mechanisms of adsorption process and the equilibrium relationship between adsorbents and adsorbate, linear and nonlinear models were modelled using Microsoft Excel 2013 and plotted using OriginPro 9, 64 bit.

2.6. Error Functions. In order to determine the best fitting of nonlinear models, four different error functions were examined by minimizing the respective error functions across the concentration and time range studied. "SOLVER ADD-IN" of Microsoft's spread sheet was used. Expressions of the error functions are given as follows [20]:

$$\chi^2 = \sum_{i=1}^{N} \frac{\left(Q_{e,\,\exp} - Q_{e,cal}\right)^2}{Q_{e,cal}},$$
$$\text{RMSE} = \sqrt{\frac{1}{n-2}\sum_{i=1}^{N}\left(Q_{e,\,\exp} - Q_{e,cal}\right)^2},$$
$$\text{SCE} = \sum_{i=1}^{N}\left(Q_{e,\,\exp} - Q_{e,cal}\right)_i^2, \quad (3)$$
$$r^2 = \frac{\sum_{i=1}^{N}\left(Q_{e,cal} - Q_{m\,\exp}\right)^2}{\sum_{i=1}^{N}\left(Q_{e,cal} - Q_{m\,\exp}\right)^2 + \left(Q_{e,cal} - Q_{m\,\exp}\right)^2},$$

where $Q_{e,exp}$ and $Q_{e,cal}$ ($mg \cdot g^{-1}$) are the equilibrium capacity of adsorption obtained from the experiment and by calculating from the model, respectively, and N is the number of data points.

3. Results and Discussion

3.1. Characterization of Adsorbent

3.1.1. Physical and Chemical Characteristics of ACs and Elemental Analysis. Physical and chemical properties of ACs $CBK_{1/1}$ and $CBZ_{1/1}$ activating are reported in Table 1. pH_{pzc} values show that surfaces of the different ACs are dominated by the basic functional group. Bulk densities of the different ACs shown in Table 1 are higher than the limit of $0.25\ g \cdot cm^{-3}$ according to American Water Works Association. Higher density gives a higher volume activity and normally indicates a better AC quality. Bulk densities of different ACs provide information on the microcrystalline structure and strong interlinking bonds. Moisture content values of different ACs obtained as presented in Table 1 are within the norm, since the traditional value for moisture content ranges from 1 to 5% by mass. Iodine number of the ACs obtained in this work is higher than limit ($500\ mg \cdot g^{-1}$), thus showing the good quality of the ACs obtained, reflecting the presence of micropores. Methylene blue number obtained and presented in Table 1 reflects the presence of mesopores on the surface of the ACs.

In Table 1, the quantity of basic groups is higher than the acidic groups on the surface of $CBK_{1/1}$ and $CBZ_{1/1}$ activated carbons, indicating that KOH and $ZnCl_2$ as activating agents for production of activated carbons by *Garcinia cola* nut shells generate carbons with higher amount of basic functional groups on their surface. The ratios of the sum of the basic groups divided by the sum of the acid groups are 1.269 (for $CBK_{1/1}$) and 1.253 (for $CBZ_{1/1}$), indicating that $CBK_{1/1}$ would be more basic than $CBZ_{1/1}$, as confirmed by the total basicity of $CBK_{1/1}$ ($3.08\ meq \cdot g^{-1}$) and $CBZ_{1/1}$ ($3.045\ meq \cdot g^{-1}$). These results follow the pH_{pzc} values, which imply that, in AC, having a higher ratio of total basic groups divided by total acid group leads to higher pH_{pzc} values. Taking into account the results of the Boehm titration and the pH_{pzc}, it can be stated that these results are in total agreement.

Elemental analyses of $CBK_{1/1}$ and $CBZ_{1/1}$ are presented in Table 1. The prepared ACs have high percentages of carbon, which in itself is a fact that justifies the use of *Garcinia cola* nut shells as a carbon source. The percentages of nitrogen and oxygen are consistent with the amount of functional groups present on activated carbons $CBK_{1/1}$ and $CBZ_{1/1}$.

3.1.2. Fourier-Transform Infrared (FTIR) Spectroscopy. Figure 3 shows that the FTIR spectra of $CBK_{1/1}$ and $CBZ_{1/1}$ are very similar to each other and different from that of the raw material, indicating that the activating agent did not influence the surface chemical group of the AC. The FTIR identified chemical groups on the surface of both ACs such as the broad peak around $3349\ cm^{-1}$ for $CBK_{1/1}$ and $CBZ_{1/1}$ which are related to OH group stretching [9]. The band obtained approximately at $1587\ cm^{-1}$ in both ACs indicates the presence of C = O stretching vibration of lactone and carbonyl groups [17]. This band can also be attributed to the C = C stretching vibration of alkene or aromatic ring [17]. The band around $1374\ cm^{-1}$ corresponds to the C–H bending vibration or C–N stretching vibration of amines or amides of nitroaromatic compounds (-NO_2).

3.1.3. X-Ray Diffraction Analysis (XRD). Figure 4 shows the XRD of ACs. In this figure, the absence of a sharp peak reveals that both ACs prepared from *Garcinia cola* nut shells are mainly amorphous structure, which is an advantageous property for well-defined porous adsorbents. However, the small sharp peak presented by the X-ray graph of $CBZ_{1/1}$ ($2\theta = 28^{\circ}$) indicates very low crystallinity may be due to the presence of zinc oxide and zinc carbide [17].

3.1.4. Thermogravimetric Analysis (TGA/DTA). TGA is performed to investigate the thermal stability of AC. The weight loss curves for $CBK_{1/1}$ and $CBZ_{1/1}$ as can be seen on the TG curves for both ACs are very similar (Figure 5).

In Figure 5, the TGA/DTA curves of both ACs suggest three typical distinct weight losses. The first weight loss of 2.016% for $CBK_{1/1}$ and 4.314% for $CBZ_{1/1}$ at temperature below 200°C corresponds to the elimination of the water content (physisorption phenomenon) in the ACs, which means that there is still physisorbed water remaining in the micropores and mesopores of the various activated carbons. The second weight loss of 20.413% for $CBK_{1/1}$ and 26.712% for $CBZ_{1/1}$ within the temperature range of 200°C–900°C may be due to the predominant decomposition of the surface chemical groups of the different ACs and the formation of H_2O, CO, and CO_2 during the calcination/activation process. In this temperature range, the decomposition of the lactone functions usually takes place between 350 and 600°C.

The third weight loss is secondary degassing which is observed above 900°C, and the resulting intermediate product linked to the carbon skeleton of the ACs involves further decomposition through the formation of residual products such as tar and oxides which are subsequently removed. Of the two ACs, the less thermally stable is $CBZ_{1/1}$, as its total mass loss is higher (37.04%), and the more thermally stable is $CBK_{1/1}$ with a lower total mass loss of 30.546%. According to the DTA curve, the thermal decomposition of the two activated carbons is dominated by an endothermic process (0°C–1250°C).

3.1.5. Scanning Electron Microscopic Images. The textural surface properties of $CBK_{1/1}$ and $CBZ_{1/1}$ were investigated by SEM (Figure 6). According to this figure, SEM images showing the prepared ACs $CBK_{1/1}$ and $CBZ_{1/1}$, respectively, illustrate an irregular and heterogeneous surface morphology with a porous structure developed and fragmented in different sizes [17]. However, it can be seen on the micrographs that the external surface of the ACs shows cracks and crevices [17]. These pores result not only from the evaporation of the chemical reagents (KOH and $ZnCl_2$) during carbonization, leaving empty spaces, but also from the

Table 1: Elemental analysis, total acidity and basicity, and physical and chemical properties.

AC	C%	H%	N%	S%	O% (diff)	Others (%)	Moisture content (%)	Bulk density ($g \cdot cm^{-3}$)	I_I ($mg \cdot g^{-1}$)	I_{MB} ($mg \cdot g^{-1}$)	Total acidity ($meq \cdot g^{-1}$)	Total basicity ($meq \cdot g^{-1}$)	pH_{pzc}
$CBK_{1/1}$	71.877	3.874	2.133	0	19.348	2.768	2.8	0.750	1065	73.177	2.428	3.08	8.324
$CBZ_{1/1}$	67.807	3.693	2.082	0	24.206	2.212	3.2	0.825	970.82	72.590	2.43	3.045	7.589

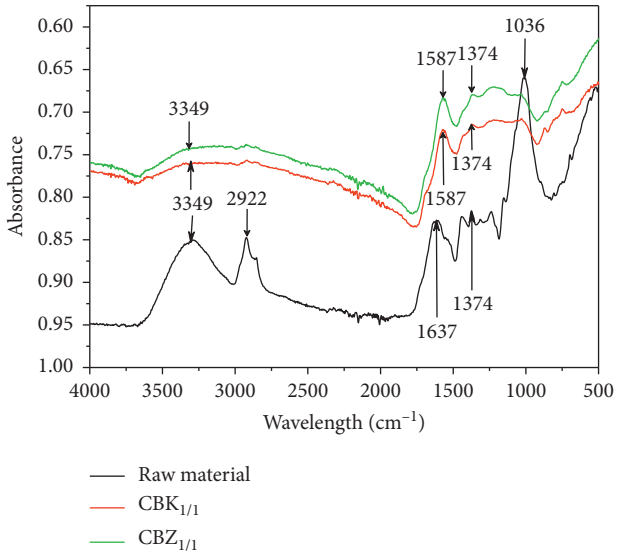

Figure 3: FTIR spectra of activated carbon ($CBK_{1/1}$ and $CBZ_{1/1}$) and raw material.

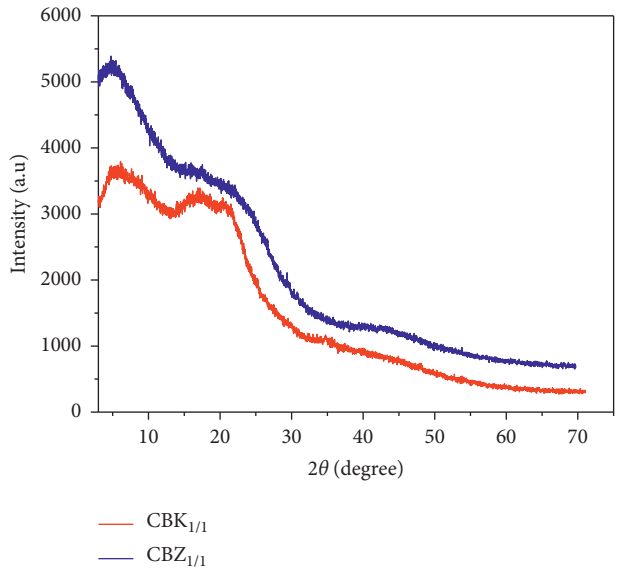

Figure 4: XRD of activated carbons: $CBK_{1/1}$ and $CBZ_{1/1}$.

degradation of the lignocellulosic material during carbonization and subsequent removal of volatile materials leaving samples with pores [17].

3.2. Batch Studies

3.2.1. Effect of pH. From Figure 7, the results show that maximum adsorption capacity is obtained for pH 2 and adsorption is favoured for $pH < pH_{pzc}$. We observe that the adsorption capacity decreases with increasing pH from 8.354 to 3.159 $mg \cdot g^{-1}$ and from 7.960 to 2.876 $mg \cdot g^{-1}$ for ACs $CBK_{1/1}$ and $CBZ_{1/1}$, respectively. It is generally known that due to the abundant presence of H^+ ions, the anionic dyes such as IC are preferentially adsorbed by the adsorbent at lower pH [21]. At that particular pH (=2) ($pH < pH_{pzc}$), protons are advantageously available for protonation of the AC surface, which increases the electrostatic interaction between the now positively charged adsorbent sites and the negatively charged sites or nucleophilic sites ($-SO_3^-$) of indigo carmine. Similar results have also been observed by several authors for the adsorption of IC [22, 23]. At the same time, IC is an anionic dye with two sulphonic acid groups and two aromatic rings; this is probably the other reason for its high removal efficiency at the low pH. A similar trend was reported by Zhao et al. [24] where they use amino acid-doped polyaniline nanotubes as adsorbent for wastewater treatment. However, increased pH ($pH > pH_{pzc}$) of the adsorbate makes it more soluble and the negative charges on the surface of the ACs increase the electrostatic repulsion force between the adsorbates (sulphonic functional group of the pollutants) and the –OH groups on the surface of the ACs due to the increase in hydroxyd ions. The electrostatic repulsion force between indigo carmine and the adsorbent promotes the decrease in adsorption capacity. A similar result was obtained from the adsorption of thymol blue onto powdered activated carbons from *Garcinia cola* nut shells impregnated with H_3PO_4 and KOH [25].

3.2.2. Effect of Contact Time. Figure 8 shows the evolution of adsorption capacity of indigo carmine as a function of the contact time at room temperature. Rapid adsorption of IC takes place in the first 5 minutes for the two ACs; this rapid phase may be attributed to rapid dye attachment on the ACs surface due to either the large amount of surface area available or to the availability of more adsorption vacant sites at the initial stage. Thereafter, the rate of adsorption deceased gradually with the progress of adsorption within 5–80 minutes for the two ACs and reached equilibrium in about 80 minutes. The adsorption capacities at these

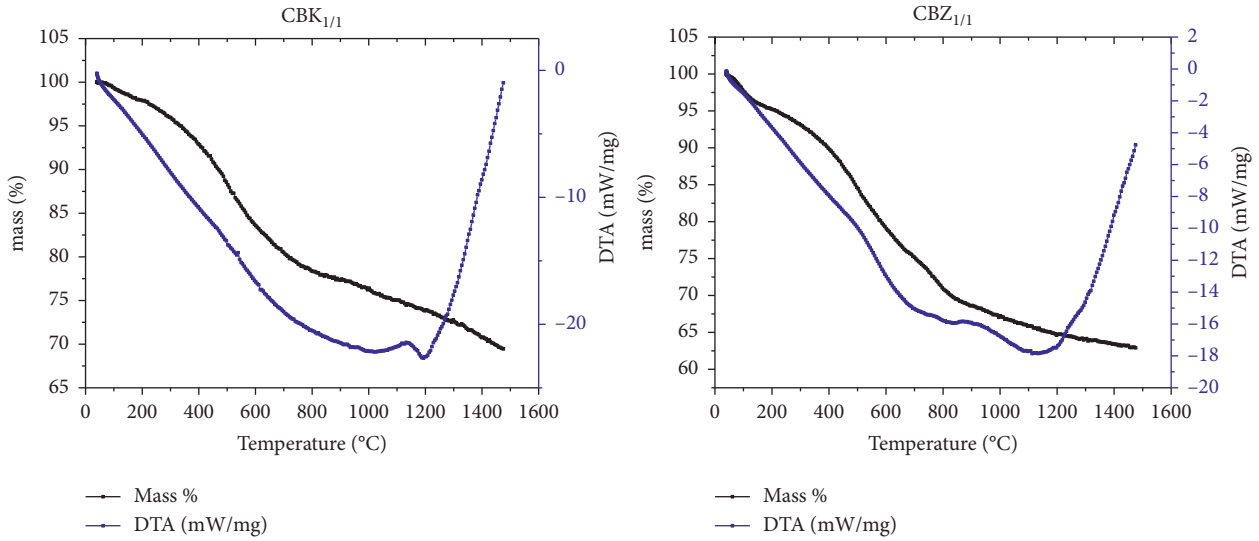

Figure 5: Thermogravimetric analysis (TGA) and differential thermogravimetric curves (DTA) of $CBK_{1/1}$ and $CBZ_{1/1}$.

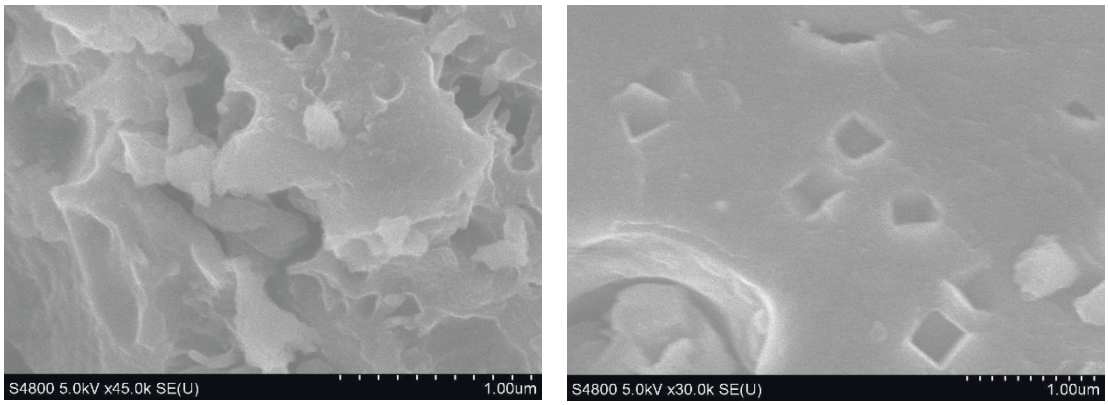

(a) (b)

Figure 6: SEM images of $CBK_{1/1}$ (a) and $CBZ_{1/1}$ (b).

equilibrium points are 8.60593 mg·g^{-1} $CBK_{1/1}$ and 8.03346 mg·g^{-1} $CBZ_{1/1}$. This can be explained by the fact that the available sites for adsorption have been greatly reduced by the indigo carmine molecules already attached there and decrease in the total adsorbent surface area and less available binding sites. The quantities adsorbed can be attributed to the $\pi-\pi$ interactions, electrostatics attractions, and formation of hydrogen bonding. In the third phase, there is no significant change in the quantity of dye adsorbed after the equilibrium time due to the saturation of the adsorption active sites by the dye molecules [26].

3.2.3. Effect of Adsorbent Mass. Effect of adsorbent mass on the removal of indigo carmine was studied, and the results of this study are shown in Figure 9. In this figure, the percentage removal of indigo carmine by $CBK_{1/1}$ and $CBZ_{1/1}$ increased as the adsorbent dosage increased. The removal percentage of indigo carmine increased from 76.8 to 97.7% and 75.1 to 92.7% for $CBK_{1/1}$ and $CBZ_{1/1}$, respectively. This is because the increase in the mass of the adsorbent leads to the increase in the adsorption sites and the contact area of each adsorbent becomes free and available for indigo carmine fixation during the adsorption process. This increase in the mass of each adsorbent further promotes the increase in their adsorption percentage. A similar trend was reported in Hameed et al. [27] for the adsorption of chromotrope dye onto activated carbons obtained from the seeds of various plants.

3.2.4. Effect of Initial Indigo Carmine Concentration. The effect of initial concentration on the adsorption of indigo carmine was investigated of 30–100 mg·L^{-1}. Figure 10 shows the quantity of indigo carmine adsorbed at equilibrium increases with the concentration from 5.814 to 11.349 mg·g^{-1} and 5.756 to 10.823 mg·g^{-1}, respectively, from $CBK_{1/1}$ and $CBZ_{1/1}$. This result can be explained by the $\pi-\pi$ interactions, electrostatic attraction, and formation of hydrogen bonding between the dyes and the surface functional groups of

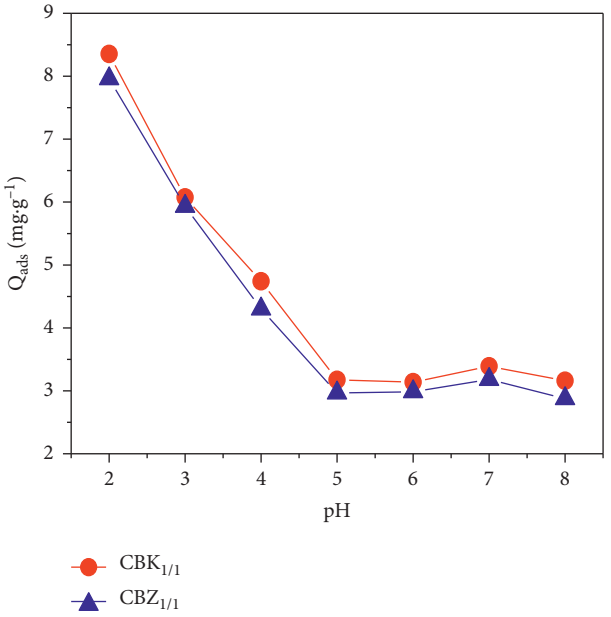

Figure 7: Effect of pH solution on the adsorption of indigo carmine. Experimental conditions: $C_0 = 50$ mg·L^{-1}; $m = 100$ mg; V = 20 mL; $t = 80$ min; speed = 200 rpm at room temperature.

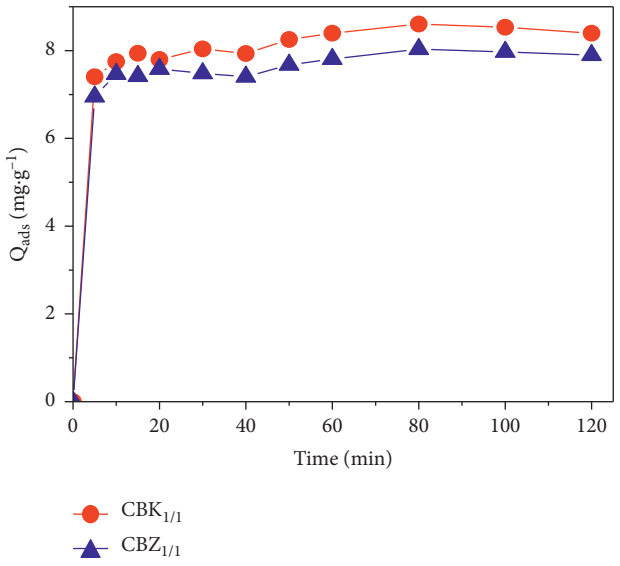

Figure 8: Effect of contact time on the adsorption of indigo carmine. Experimental conditions: $C_0 = 50$ mg·L^{-1}; $m = 100$ mg; V = 20 mL; pH = 2; speed = 200 rpm at room temperature.

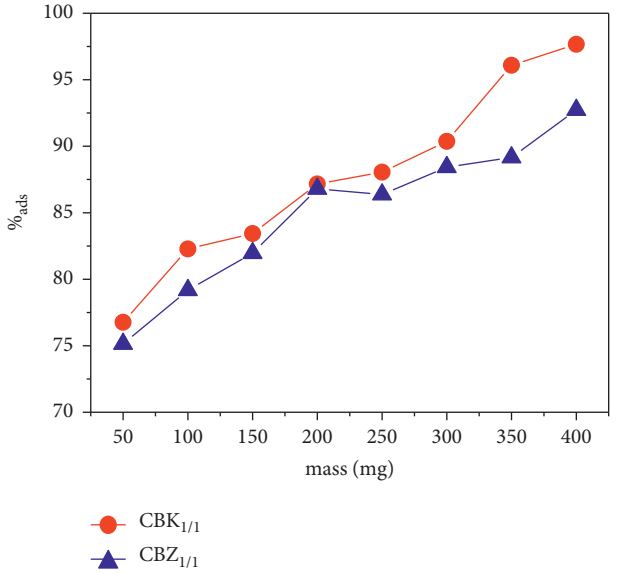

Figure 9: Effect of adsorbent dosage on the adsorption of indigo carmine. Experimental conditions: $C_0 = 50$ mg·L^{-1}; V = 20 mL; pH = 2; $t = 80$ min; speed = 200 rpm at room temperature.

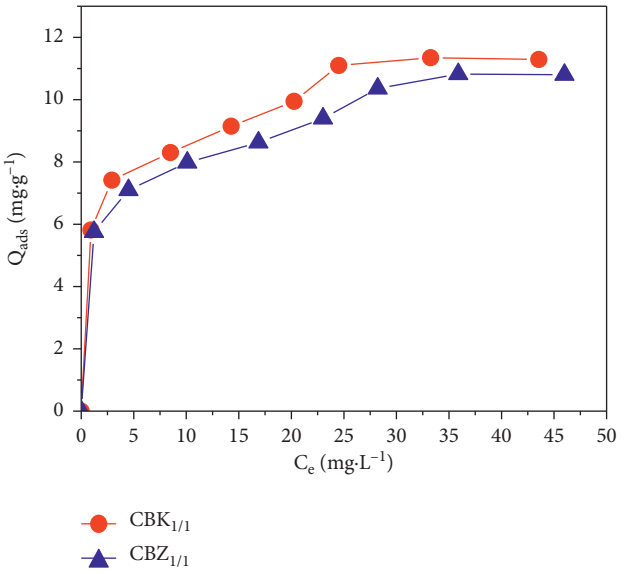

Figure 10: Effect of initial concentration on the adsorption of indigo carmine. Experimental conditions: $m = 100$ mg; V = 20 mL; pH = 2; $t = 80$ min; speed = 200 rpm at room temperature.

activated carbons on the one hand and the difference in the pore size of these carbons on the other hand. This can also be explained by the fact that increasing the initial concentration of indigo carmine would increase the driving force of mass transfer and, consequently, the speed at which indigo carmine molecules pass from the solution to the surface of the ACs [28]. In this figure, we observe a saturation of the adsorption sites which is progressively increasing until reaching a plateau caused by the formation of monolayers on the surface of each adsorbent. The isotherm forms of CBK$_{1/1}$ and CBZ$_{1/1}$ have been classified as type *L* which can be better explained by the Langmuir, Freundlich, and Temkin models that show a relatively high affinity between the adsorbate and adsorbent.

3.2.5. Effect of Ionic Strength. The effect of ionic strength on adsorption of indigo carmine onto CBK$_{1/1}$ and CBZ$_{1/1}$ was studied in the NaCl solutions with concentrations ranging from 0.01 to 0.06 mol·L^{-1}, and the results are illustrated in Figure 11. When the ionic strength increased, the adsorption

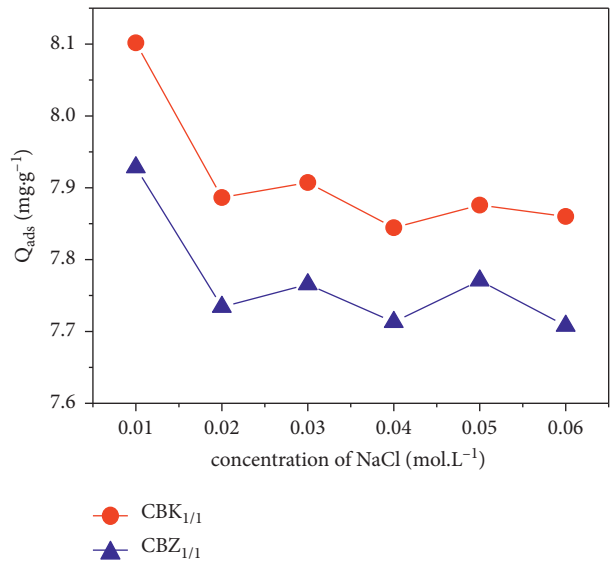

Figure 11: Effect of ionic strength on the adsorption of indigo carmine. Experimental conditions: $C_0 = 50$ mg·L^{-1}; $m = 100$ mg; V = 20 mL; pH = 2; $t = 80$ min; speed = 200 rpm at room temperature.

Table 2: Linear and nonlinear kinetic models.

Kinetic models	Linear and nonlinear forms	Equation number	References
Pseudofirst order	$dQ_t/dt = K_1(Q_e - Q_t)$	(4)	[30]
	$\ln(Q_e - Q_t) = \ln Q_e - K_1 t$	(5)	
	$Q_t = Q_e(1 - e^{-K_1 t})$	(6)	
Pseudosecond order	$dQ_t/dt = K_2(Q_e - Q_t)^2$	(7)	[31]
	$t/Q_t = (1/K_2 Q_e^2) + (t/Q_e)$	(8)	
	$Q_t = K_2 Q_e^2 t/(1 + K_2 Q_e t)$ and $h = K_2 Q_e{}^2$	(9)	
Avrami	$\ln(\ln(Q_{exp}/Q_{exp} - Q_t)) = n_{AV} \ln K_{AV} - n_{AV} \ln t$	(10)	[32]
	$Q_t = Q_e\{1 - \exp[-(K_{AV}t)]^{n_{AV}}\}$	(11)	
Intraparticle diffusion	$Q_t = K_{int} t^{1/2} + C$	(12)	[33]
Boyd	$B_t = -0,4977 - \ln(1 - F)$	(13)	[18]
	$F = (Q_t/Q_e)$	(14)	
	$B = \pi^2 D_i/r^2$	(15)	

capacity of indigo carmine decreased (from 8.102 to 7.860 mg·g^{-1} and 7.928 to 7.708 mg·g^{-1}) for CBK$_{1/1}$ and CBZ$_{1/1}$, respectively. This result can be explained by the fact that the surface of the ACs becomes difficult to access by indigo carmine when the amount of NaCl salt in solution increases. Consequently, the adsorption capacity of indigo carmine decreases. This result is in agreement with the literature, which reports that when the electrostatic attraction forces between the surface of an adsorbent and the ions of an adsorbate are attractive, the increase in ionic strength thus decreases the adsorption capacity [29].

3.3. Adsorption Kinetics. In this work, the data from the kinetic experiments were analyzed using the different linear and nonlinear kinetic models presented in Table 2.

The linear and nonlinear regression graphs of adsorption kinetics for indigo carmine adsorption onto both ACs are shown in Figures 12 and 13, respectively, and the corresponding constants are summarized in Tables 3 and 4.

According to Table 3, the data linear kinetic model indicates that the pseudo-second order model is perfectly appropriate to describe the adsorption kinetics of indigo carmine and on both ACs with a high correlation coefficient ($R^2 \geq 0.9993$). Moreover, it can be observed that the experimental $Q_{e,exp}$ values obtained during the equilibrium adsorption process are close to the $Q_{e,cal}$ values calculated from the pseudo-second order model, which indicates that the adsorption of indigo carmine on both ACs is a process dominated by the interaction π–π [33]. The values of the initial rate of reaction and the reaction half time determined from pseudo-second order model confirm that the accumulation kinetics of indigo carmine is faster at the surface of AC CBK$_{1/1}$ than at the surface of CBZ$_{1/1}$. Figure 12(d) shows that the plot of $Q_t = f(t^{1/2})$ is not a straight line through the origin of the marker. This indicates that the intraparticle diffusion is not the limiting step or the only rate control step in the adsorption process of indigo carmine on ACs. In this case, other kinetic models can also control the adsorption rate to describe other adsorption mechanisms.

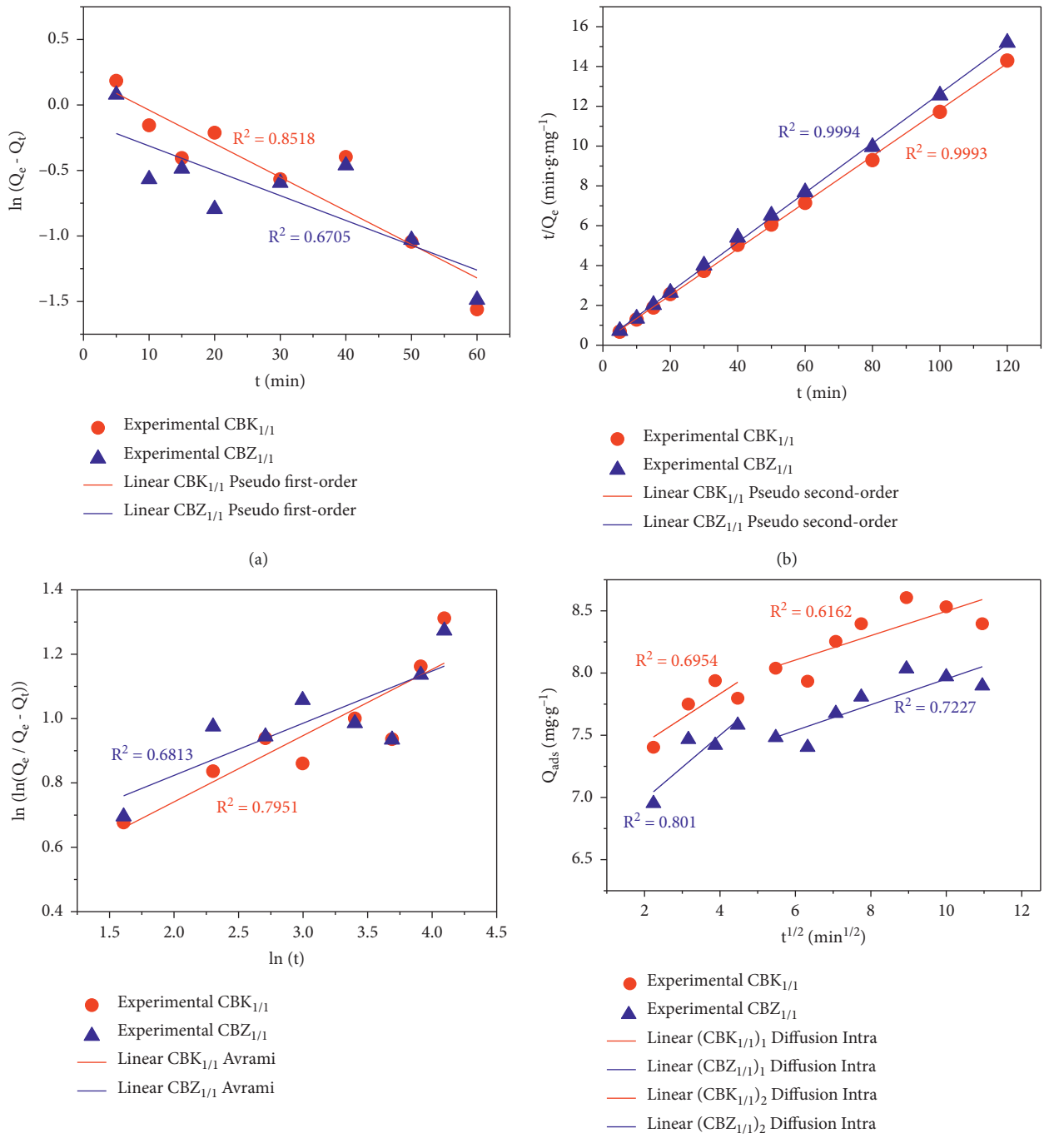

Figure 12: Continued.

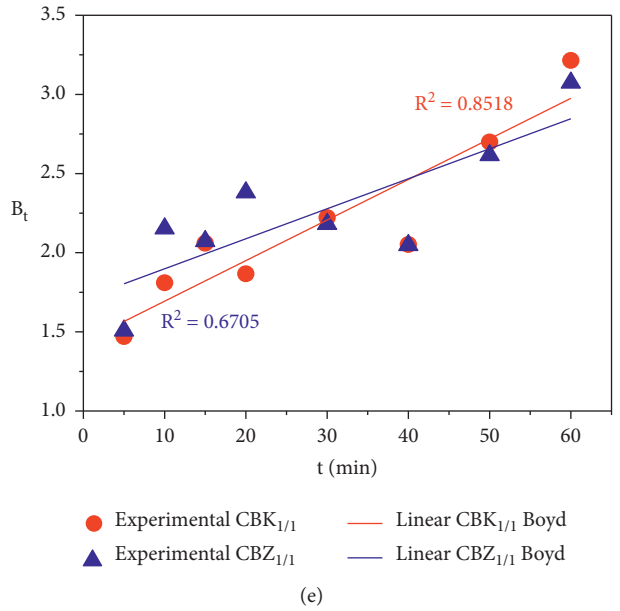

Figure 12: Linear regression of adsorption kinetics of (a) pseudofirst order, (b) pseudosecond order, (c) Avrami, (d) intraparticle diffusion, and (e) Boyd.

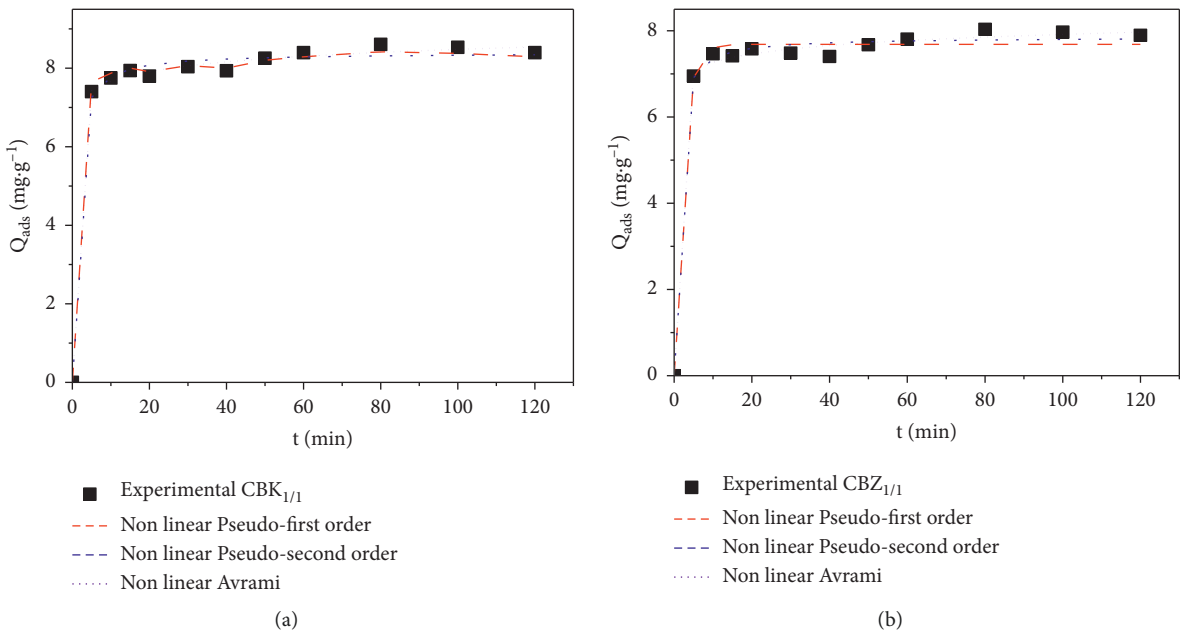

Figure 13: Nonlinear regression of adsorption kinetics.

As shown in Figure 12(d), the adsorption of indigo carmine on ACs forms two straight line segments over the entire time interval, meaning that this adsorption process can be controlled by at least two mechanisms occurring simultaneously [33]. This can be attributed to the difference in mass transfer rate between the initial stage and the final stage in ACs. It can be said that at least two types of pores, namely, micropores and mesopores, are involved in the adsorption of indigo carmine. The analysis of Table 4 shows that the first step is faster than the second since $K_{id1} > K_{id2}$. However, the values of boundary layer thickness C for each linear portion not approaching zero ($C_2 > C_1$) corresponding to the increase in boundary layer thickness indicate that intraparticle diffusion is not the only step in controlling the adsorption rate in all stages [34].

Figure 12(e) shows that the Boyd model lines do not pass through the origin of the graph, meaning that external mass transfer primarily governs the rate controlling step at the

Table 3: Linear and nonlinear parameters of kinetic models for adsorption of IC onto ACs.

Models	Linear pseudofirst order	Linear pseudosecond order	Linear Avrami	Nonlinear pseudofirst order	Nonlinear pseudosecond order	Nonlinear Avrami
CBK1/1						
Parameter $Q_{e,exp} = 8.605$ $(mg{\cdot}g^{-1})$	$Q_{e,\ cal} = 1.243$ $(mg{\cdot}g^{-1})$ $K_1 = 0.0256$ (min^{-1})	$Q_{e,\ cal} = 8.584$ $(mg{\cdot}g^{-1})$ $K_2 = 0.07615$ $(g{\cdot}mg^{-1}{\cdot}min^{-1})$ $h = 5.6107$ $(mg{\cdot}g^{-1}{\cdot}min^{-1})$	— $K_{Av} = 0.20202$ (min^{-1}) $n_{Av} = -0.20591$	$Q_{e,\ cal} = 14.243$ $(mg{\cdot}g^{-1})$ $K_1 = 0.104$ (min^{-1})	$Q_{e,cal} = 8.396$ $(mg{\cdot}g^{-1})$ $K_2 = 0.151$ $(g{\cdot}mg^{-1}{\cdot}min^{-1})=$ $h = 10{,}644$ $(mg{\cdot}g^{-1}{\cdot}min^{-1})$	$Q_{e,cal} = 12.121$ $(mg{\cdot}g^{-1})$ $K_{Av} = 0.104$ (min^{-1}) $n_{Av} = 0.079$
r2				0.762	0.752	0.884
$\chi 2$				0.022	0.043	0.020
RMSE				0.141	0.199	0.134
SCE				0.179	0.355	0.163
CBZ1/1						
Parameter Qe,exp = 8.034 (mg g–1)	$Q_{e,cal} = 0.8843$ $(mg{\cdot}g^{-1})$ $K_1 = 0.01896$ (min^{-1})	$Q_{e,\ cal} = 8.0282$ $(mg{\cdot}g^{-1})$ $K_2 = 0.0847$ $(g{\cdot}mg^{-1}{\cdot}min^{-1})$ $h = 5.4591$ $(mg{\cdot}g^{-1}{\cdot}min^{-1})$	— $K_{Av} = 0.46717$ (min^{-1}) $n_{Av} = -0.82541$	$Q_{e,\ cal} = 7.686$ $(mg{\cdot}g^{-1})$ $K_1 = 0.460$ (min^{-1})	$Q_{e,\ cal} = 7.853$ $(mg{\cdot}g^{-1})$ $K_2 = 0.187$ $(g{\cdot}mg^{-1}{\cdot}min^{-1})$ $h = 11.532$ $(mg{\cdot}g^{-1}{\cdot}min^{-1})$	$Q_{e,\ cal} = 11.485$ $(mg{\cdot}g^{-1})$ $K_{Av} = 0.104$ (min^{-1}) $n_{Av} = 0.067$
r2				0.525	0.731	0.810
$\chi 2$				0.063	0.035	0.025
RMSE				0.231	0.173	0.144
SCE				0.482	0.268	0.187

Table 4: Intraparticle diffusion and Boyd parameters for adsorption of IC onto ACs.

Models	Constants	Values
$CBK_{1/1}$		
Linear intraparticle diffusion	K_{id1} $(mg{\cdot}g^{-1}{\cdot}min^{-1/2})$	0.197
	K_{id2} $(mg{\cdot}g^{-1}{\cdot}min^{-1/2})$	0.09814
	C_1	7.0454
	C_2	7.5157
Linear Boyd	B (min^{-1})	0.02563
	$Di \times 10^{-9}$ $(cm^2{\cdot}s^{-1})$	1.083
$CBZ_{1/1}$		
Linear intraparticle diffusion	K_{id1} $(mg{\cdot}g^{-1}{\cdot}min^{-1/2})$	0.2578
	K_{id2} $(mg{\cdot}g^{-1}{\cdot}min^{-1/2})$	0.1035
	C_1	6.4687
	C_2	6.9168
Linear Boyd	B (min^{-1})	0.01896
	$Di \times 10^{-9}$ $(cm^2{\cdot}s^{-1})$	0.8012

Table 5: Isotherm models.

Parameters	Isotherms	Nonlinear forms	Equation number	References
Two	Langmuir	$Q_e = Q_m K_L C_e / 1 + K_L C_e$	(16)	[36]
		And $R_L = 1/(1 + K_L C_0)$	(17)	
	Freundlich	$Q_e = K_f C_e^{1/n}$	(18)	[37]
	Temkin	$Q_e = (RT/\Delta Q)\mathrm{In}(\mathrm{ACe})$	(19)	[38]
	Halsey	$Q_e = \exp((\mathrm{InK_H} - \mathrm{InC_e})/n_H)$	(20)	[39]
	Fritz–Schlunder III	$Q_e = Q_{mFS} K_{FS} C_e / (1 + Q_{mFS} C_e^{mFS})$	(21)	[40]

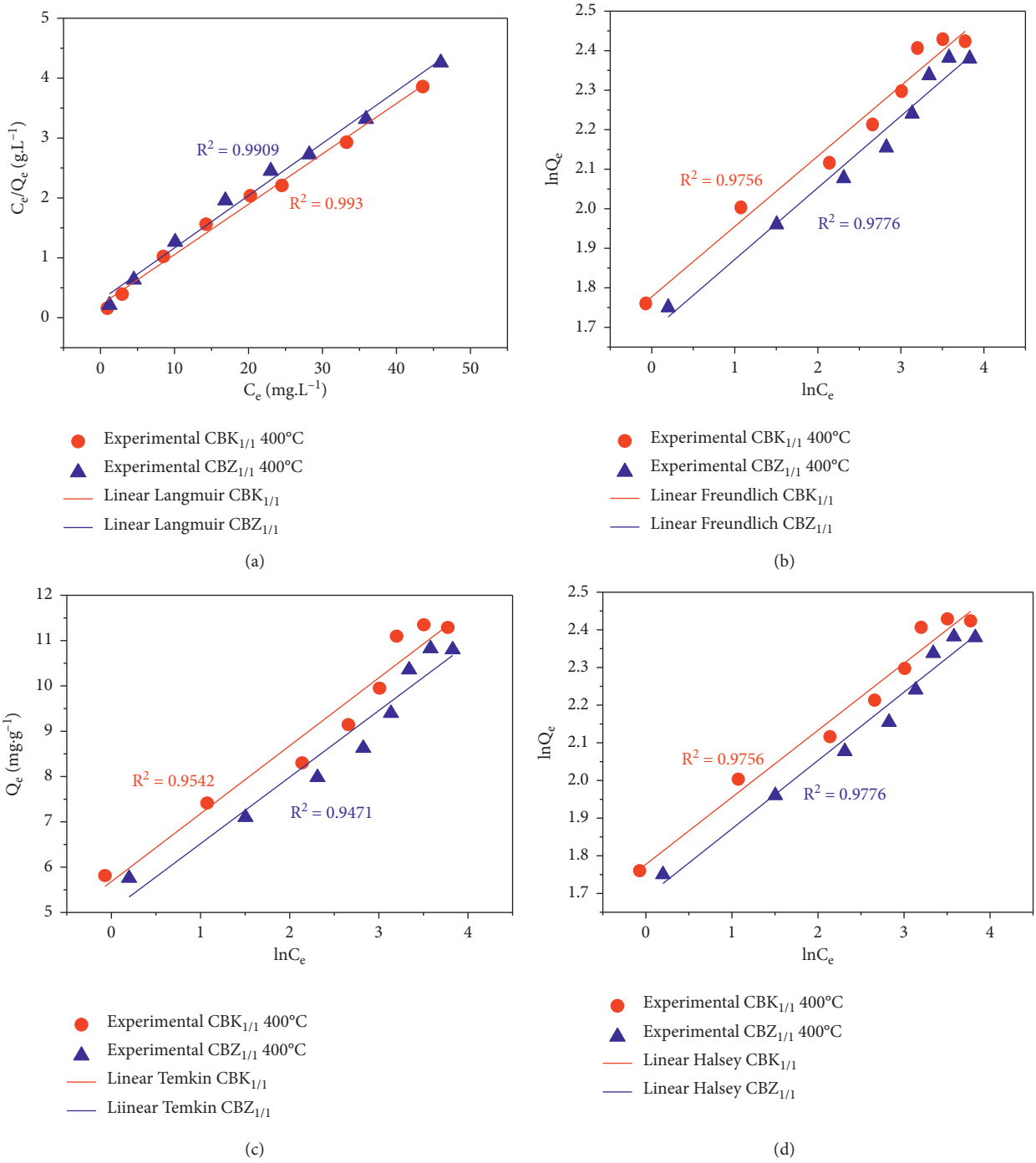

Figure 14: Continued.

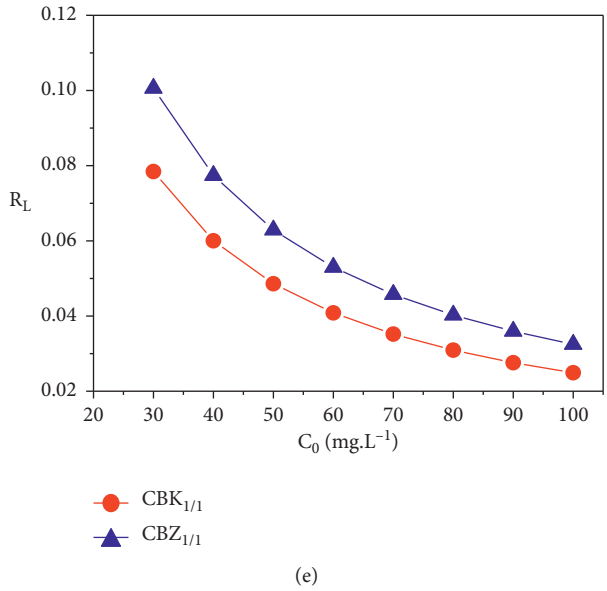

(e)

Figure 14: Linear regression of isotherm models of (a) Langmuir, (b) Freundlich, (c) Temkin, (d) Halsey, and (e) separation factor graphs.

initial stages [18, 35]. In Table 4, the low values of the correlation coefficient obtained do not make it possible in this case to validate Boyd's model.

Based on the nonlinear regression data of the different models shown in Table 3 and on the low values obtained from SCE and other error functions, it can be concluded that the retention kinetics of indigo carmine are best described by the nonlinear Avrami model. The values of the Avrami exponent $n_{Av} < 1$ show that the adsorption mechanism follows a multiple kinetic order during the adsorption process of indigo carmine on the two ACs. Thus, in this work, the pseudo-first order shows a multilayer adsorption on the surface of the adsorbent based on a weak interaction between the adsorbate and the adsorbent like the Van der Waals forces and the pseudo-second order model allows us to say that the interaction π–π [33] also intervenes in this adsorption process of indigo carmine on the two ACs, thus showing an adsorption of chemical nature.

3.4. Adsorption Isotherms. Adsorption isotherms can contribute to elucidating adsorption mechanisms. In this work, data from the isotherm experiments were analyzed using the different linear and nonlinear kinetic models presented in Table 5.

The linear and nonlinear regression graphs of adsorption isotherms for indigo carmine adsorption onto both ACs are shown in Figures 14 and 15, respectively, and the corresponding constants are summarized in Tables 6 and 7.

The linear regression and separation factor graphs of adsorption isotherms obtained for indigo carmine adsorption onto both ACs are shown in Figure 14. The corresponding constants obtained from the linear regressions are presented in Table 6. According to this figure, the values of correlation coefficient (R^2) in the Langmuir model were closer to unity showing fitness of model on the adsorption experiment. This result indicates that adsorption of indigo carmine could take place at homogeneous adsorption sites and that monolayer adsorption occurs on the surface of the adsorbent [41]. The values of the separation factor falling between 0 and 1 (Figure 14(e)) show a favorable adsorption of IC by the two ACs.

Parameters calculated for Freundlich and Halsey isotherms by employing their linear and nonlinear forms are given in Tables 6 and 7. The results show that the Freundlich and Halsey isotherms have a very good coefficient of determination ($r^2 > 0.96$) and very low values of the error functions (χ^2, RMSE, and SCE), thus better describing the phenomenon of indigo carmine adsorption. This assumes that the adsorbent surface is heterogeneous with a non-uniform distribution of the heat of adsorption over this surface showing multilayer adsorption [42]. The values of 1/n evaluated from the Freundlich model are less than unity, meaning that adsorption is favorable for dye [43] and physical process is favorable [44]. This confirms the heterogeneity of the adsorbents as found by the SEM.

Maximum adsorption capacities were obtained by the nonlinear Fritz–Schlunder III model and are 19.019 mg·g^{-1} and 18.299 mg·g^{-1} for CBK$_{1/1}$ and CBZ$_{1/1}$, respectively. The Fritz–Schlunder model exponent m_{FS} value obtained by the nonlinear Fritz–Schlunder III isotherm of less than 1 means that the adsorption of indigo carmine by the two ACs cannot be reduced to the Langmuir isotherm showing that adsorption takes place on heterogeneous surfaces.

3.5. Possible Adsorption Mechanisms. Surface characteristics of adsorbents play an important role in adsorption processes [49]. Thus, the interaction of any molecule in the adsorption process is strongly influenced by the presence of functional

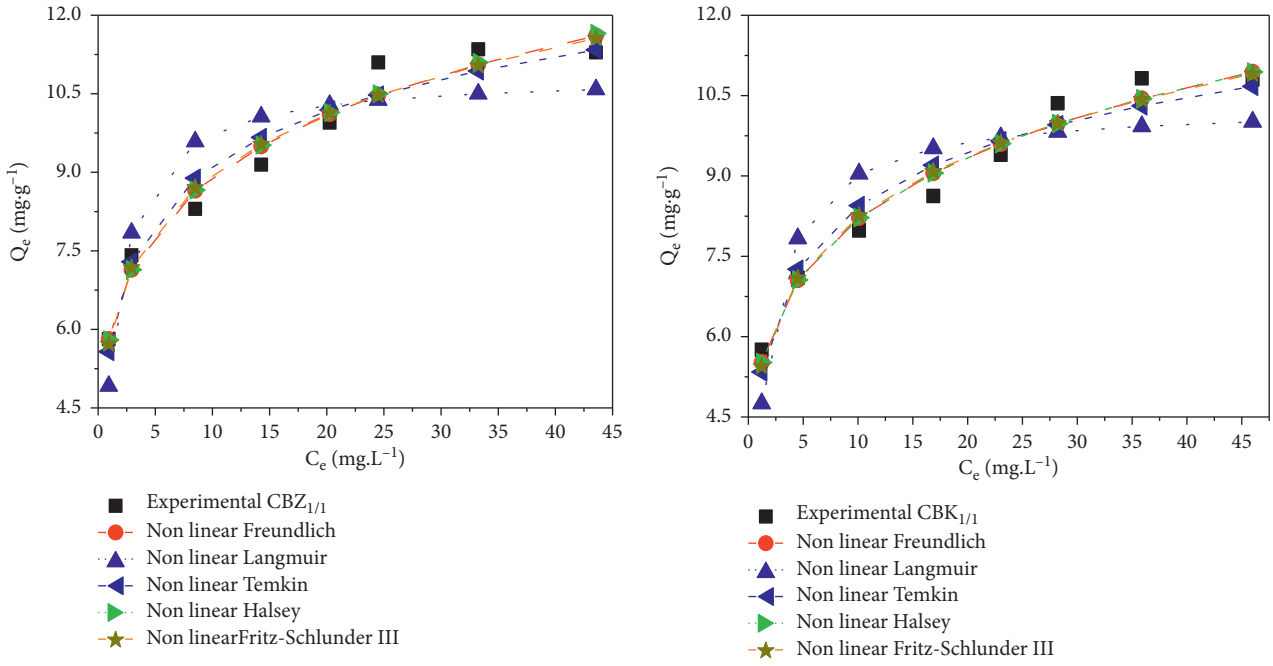

Figure 15: Nonlinear regression of adsorption isotherm models.

Table 6: Linear parameters of isotherm models for adsorption of IC onto ACs.

Isotherms	Constants	Values	r^2	χ^2	RMSE	SCE
CBK$_{1/1}$						
Langmuir	Q_m (mg·g^{-1})	11.905	0.8484	2.582	1.30822	10.2687
	K_L (L·mg^{-1})	0.3916				
Freundlich	K_F(L·g^{-1})	5.9133	0.9657	0.095	0.39434	0.93302
	1/n	0.178				
Temkin	ΔQ (J·mol^{-1})	1653.04	0.9542	0.138	0.4666	1.3064
	A (L·g^{-1})	44.2992				
Halsey	K_H	4.6×10^5	0.9668	0.095	0.39434	0.93304
	n_H	−5.618				
CBZ$_{1/1}$						
Langmuir	Q_m (mg·g^{-1})	11.455	0.8387	2.6225	1.2483	9.3496
	K_L (L·mg^{-1})	0.298				
Freundlich	K_F(L·g^{-1})	5.4211	0.9699	0.0724	0.3366	0.679903
	1/n	0.1814				
Temkin	ΔQ (J·mol^{-1})	1686.5	0.9471	0.1477	0.45710	1.2537
	A (L·g^{-1})	31.094				
Halsey	K_H	9×10^5	0.9699	0.0724	0.3366	0.67992
	n_H	−5.513				

groups on the surface of the adsorbent and also by the pH of the adsorbate solution [50]. The probable mechanism of adsorption of the dye on carbon is presented in Figure 16.

The equilibrium study showed the possibility of multilayer adsorption, in which the adsorbate-adsorbent interactions are carried out up to the saturation of the monolayer. Furthermore, based on the chemical structure of the adsorbent surface, the dyes, and considering the condition of the pH of the medium below the pH of zero charge point, which leads to a positively charged adsorbent surface, we can say that, in the adsorption process, there occurs the electrostatic interaction (attraction) between the protonated groups under acidic conditions (e.g., $-OH_2^+$ and $-COOH_2^+$) and anionic sulphonate groups ($-SO_3^-$) of the dye on the one hand. If electrostatic interaction dominates the adsorption process of IC in aqueous solution, the ACs will exhibit lower adsorption capacity due to electrostatic repulsion between the adsorbent and the adsorbate at pH 2 because the functional groups

Table 7: Nonlinear parameters of isotherm models for adsorption of IC onto ACs.

	Isotherms	Constants	Values	r^2	χ^2	RMSE	SCE
Nonlinear methods			$CBK_{1/1}$				
	Langmuir	Q_m ($mg{\cdot}g^{-1}$)	10.853	0.836	0.619	0.9426	5.3307
		K_L ($L{\cdot}mg^{-1}$)	0.8901				
	Freundlich	K_F ($L{\cdot}g^{-1}$)	5.8875	0.966	0.094	0.3937	0.9299
		1/n	0.1799				
	Temkin	ΔQ ($J{\cdot}mol^{-1}$)	1652.9	0.954	0.138	0.4666	1.3064
		A ($L{\cdot}g^{-1}$)	44.293				
	Halsey	K_H	5×10^{-5}	0.968	0.094	0.3937	0.9299
		n_H	−5.5593				
	Fritz–Schlunder III	Q_{mFS} ($mg{\cdot}g^{-1}$)	19.019	0.966	0.0998	0.4031	0.9753
		K_{FS} ($L{\cdot}mg^{-1}$)	6.113				
		m_{FS}	0.831				
			$CBZ_{1/1}$				
	Langmuir	Q_m ($mg{\cdot}g^{-1}$)	10.320	0.810	0.672	0.9383	5.2825
		K_L ($L{\cdot}mg^{-1}$)	0.6993				
	Freundlich	K_F ($L{\cdot}g^{-1}$)	5.3160	0.973	0.072	0.3297	0.6521
	Temkin	1/n	0.1885	0.947	0.148	0.4571	1.2537
		ΔQ ($J{\cdot}mol^{-1}$)	1686.5				
	Halsey	A ($L{\cdot}g^{-1}$)	31.095	0.973	0.072	0.3297	0.6521
		K_H	0.0001				
		n_H	−5.3076				
	Fritz–Schlunder III	Q_{mFS} ($mg{\cdot}g^{-1}$)	18.299	0.970	0.0856	0.3517	0.7423
		K_{FS} ($L{\cdot}mg^{-1}$)	5.4982				
		m_{FS}	0.8204				

Table 8: Comparison of adsorption capacity of indigo carmine with other adsorbents.

Adsorbents	Quantity adsorbed ($mg{\cdot}g^{-1}$)	Reference
Crab shell chitosan	96.15	[45]
Peanut shell activated carbon	82.64	[45]
LDH nanoparticles	55.5	[46]
AC (KOH)	13.405	[7]
AC (H_3PO_4)	5.089	[7]
Chitin	5.78	[47]
Brazil nut shell	1.09	[48]
PKSAC	11.025	[21]
PKSAC/BVA	12.642	[21]
$CBK_{1/1}$	19.019	Present study
$CBZ_{1/1}$	18.299	Present study

($-OH_2^+$ and $-COOH_2^+$) of the ACs (pHpzc = 8.324 for $CBK_{1/1}$; 7.589 for $CBZ_{1/1}$) and indigo carmine (pKa = 12.2) are positively charged in such an acidic environment. This does not correspond to the experimental results obtained at pH = 2; we have a high adsorption capacity. On the other hand, intermolecular hydrogen bonding of dye molecules generally leads to multilayer adsorption [24]. Adsorption of indigo carmine follows the multilayer adsorption pattern heterogeneous surfaces until saturation of the monolayer. This indicates that hydrogen bonding could be the dominant force for adsorption accompanied by the $\pi-\pi$ interaction between the aromatic rings of the dye and the ACs, which is also considered responsible for the adsorption process [51]. Electrostatic attraction also plays an important role in indigo carmine adsorption.

3.6. Desorption. In this study, the desorbing agents such as H_2O, NaOH, and H_2SO_4 4×10^{-2} $mol{\cdot}L^{-1}$ were used to regenerate both ACs. The results presented in Figure 17 show that the higher desorption percentage, 61.259% for IC $CBK_{1/1}$ and 55.08% for IC $CBZ_{1/1}$, is obtained in NaOH solution. This result can be explained by the phenomenon of anionic exchange between OH^- of NaOH solution and the activated carbons charged by indigo carmine. However, the low percentage of desorption obtained with $CBZ_{1/1}$ compared to $CBK_{1/1}$ is due to the strong bond formed between the IC and the surface of activated carbon $CBZ_{1/1}$ [18, 52]. A similar result was obtained by Ngaha et al. [19] in the indigo carmine and 2,6-dichlorophenolindophenol removal using cetyltrimethylammonium bromide-modified palm oil fiber.

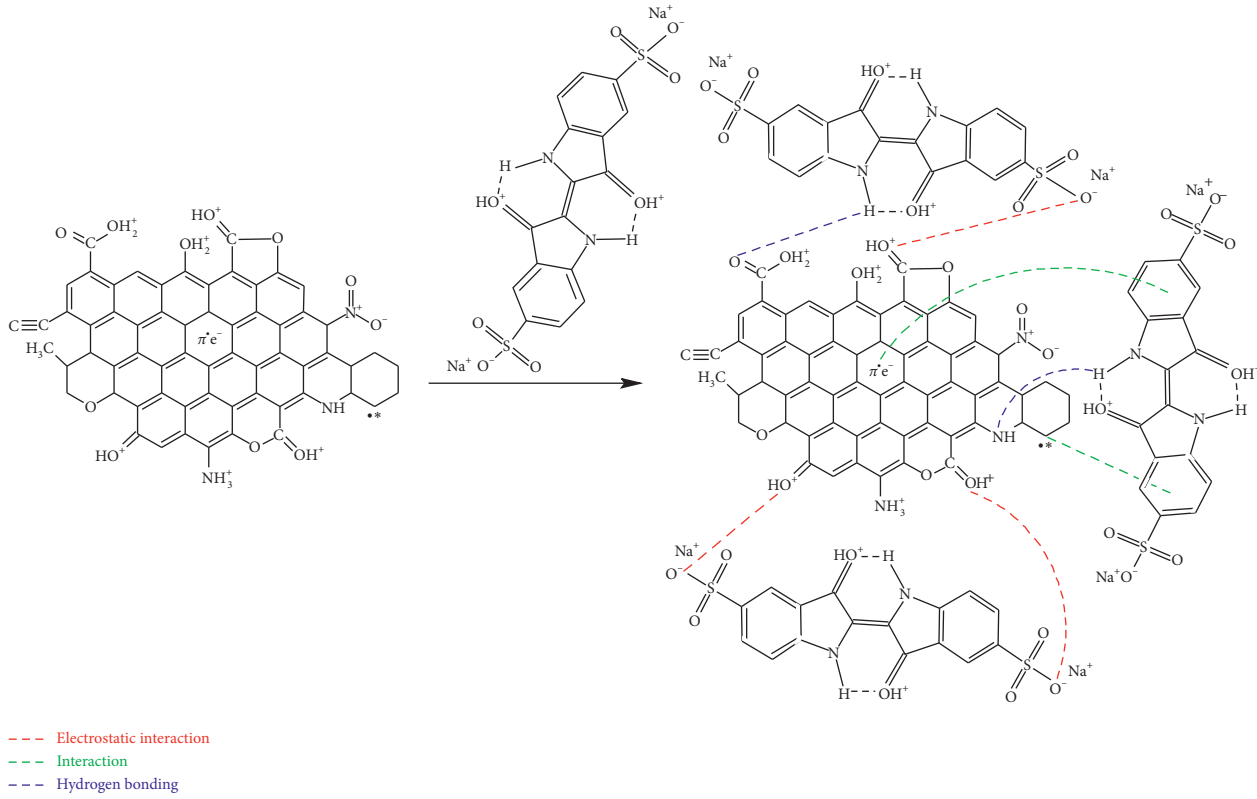

Figure 16: Probable mechanism involved during adsorption of IC by activated carbons.

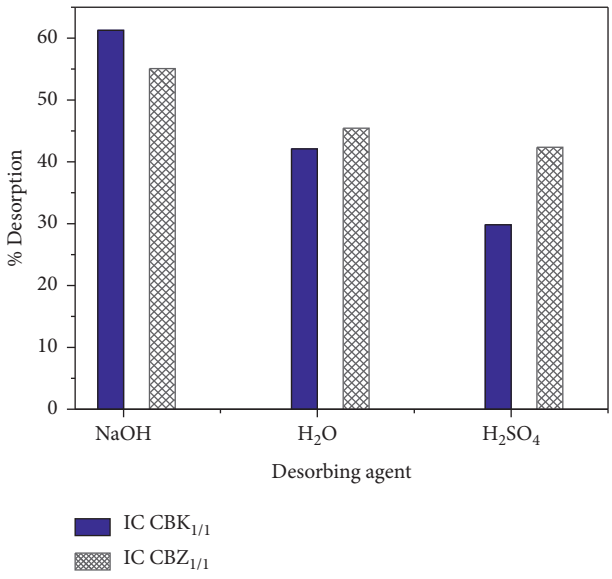

Figure 17: Percentage of desorption obtained onto different ACs after adsorption of IC. Experimental conditions: 50 mg; $t = 80$ min; $v = 200$ rpm; V = 10 mL, at room temperature.

4. Conclusion

In this study, activated carbons were prepared from *Garcinia cola* nut shell by chemical activation using KOH and $ZnCl_2$. They were used for removal of indigo carmine from aqueous solution by the batch process. SEM and N_2 adsorption-desorption analysis showed that the surfaces of the ACs were heterogeneous and contained with micropores and mesopores. The adsorption process of IC onto the adsorbents was strongly dependent on the pH of the dye solution, contact time, adsorbent dosage, initial concentration of IC, and the presence of ionic strength. Linear and nonlinear kinetic and equilibrium isotherm models were applied to the adsorption of IC onto activated carbons obtained. Nonlinear kinetic models better describe the mechanism of adsorption process than linear kinetic models which show that the adsorption mechanism follows a multiple kinetic order during the adsorption process of indigo carmine on the ACs according to Avrami exponent n_{Av} lower than 1. Nature and the mechanism of the adsorption processes were studied by employing the intraparticle diffusion model and Boyd plot. External mass transfer primarily governs the rate controlling step at the initial stages for the adsorption of the IC. Linear and nonlinear equilibrium isotherm models show that IC adsorption is done on heterogeneous surface and forms nonideal monolayer. This heterogeneity was also confirmed by the constants of Fritz–Schlunder III. Comparison between linear and nonlinear isotherm models with two parameters shows that transformations of nonlinear isotherm equations to linear forms implicitly alter their error structure. Nonlinear forms better describe adsorption process than linear forms. Desorption using NaOH solution as the desorbing agent recovers a maximum quantity of IC and considers the reuse of activated carbons. In future work, we plan to study the life cycle of the biomass used, to use these activated carbons for biogas purification, and finally to study

the influence of the NaOH concentration on the desorption percentage and the desorption kinetics of the two activated carbons.

Data Availability

The data used to support the findings of this study are available from the corresponding author upon request and have been deposited in the Mendeley repository (https://www.mendeley.com/reference-manager/library/all-references/).

Conflicts of Interest

The authors declare that they have no conflicts of interest.

Acknowledgments

This work was funded by the Government of Cameroon by Research Modernization grants to researchers of higher education. The authors are grateful for technical assistance rendered by the researchers of Materials and Process Engineering Team/RU-NOGEE of the Department of Chemistry, Faculty of Science, University of Dschang, Cameroon. They are also grateful to Kamdem Tamo Arnaud of the Freiburg Materials Research Center (FMF), University of Freiburg, Stefan Meier Strasse 21, 79104, Freiburg, Germany, and Doungmo Giscard of the Institute of Inorganic Chemistry, Christian-Albrechts-Universität zu Kiel, Max-Eyth-Straβe 2, 24118 Kiel, Germany.

References

[1] R. D. C. Soltani, A. Khataee, M. Safari, and S. Joo, "Preparation of bio-silica/chitosan nanocomposite for adsorption of a textile dye in aqueous solutions," *International Biodeterioration & Biodegradation*, vol. 85, pp. 383–391, 2013.

[2] J. Shen, X.-L. Wang, Y.-X. Niu, Y.-G. Wang, G. Liu, and Q.-T. Sheng, "Removal of phenol by powdered activated carbon prepared by residue extracted from coal gasifcation tar residue," *Environmental Technology*, vol. 10, pp. 1–8, 2017.

[3] R. Connor, A. Renata, C. Ortigara et al., "The united nations world water development report 2017," 2017, https://wedocs.unep.org/20.500.11822/20448.

[4] V. K. Gupta and I. Ali, "Environmental water," *Advances in Treatment, Remediation and Recycling*, Elsevier, Oxford, UK, 2013.

[5] J.-C. Saurin, "Role of chromoendoscopy for the management of colorectal neoplasia," *Gastroentérologie Clinique et Biologique*, vol. 33, no. 10-11, pp. 1–6, 2009.

[6] P. Himanshu and R. Vashi, "Decolonization of Dyeing Mill waste water by adsorption and coagulation," *E-Journal of chemistry*, vol. 7, pp. 1468–1476, 2010.

[7] A. N. Odogu, K. Daouda, B. B. P. Desiré, N. J. Nsami, and K. J. Mbadcam, "Removal of indigo carmine dye (IC) by batch adsorption method onto dried cola nut shells and its active carbon from aqueous medium," *International Journal of Engineering Sciences & Research Technology*, vol. 5, pp. 874–887, 2016.

[8] H. N. Tran, S.-J. You, T. V. Nguyen, and H.-P. Chao, "Insight into the adsorption mechanism of cationic dye onto biosorbents derived from agricultural wastes," *Chemical Engineering Communications*, vol. 204, no. 9, pp. 1020–1036, 2017.

[9] S. Rovani, M. T. Censi, S. L. Pedrotti, E. C. Lima, R. Cataluña, and A. N. Fernandes, "Development of a new adsorbent from agro-industrial waste and its potential use in endocrine disruptor compound removal," *Journal of Hazardous Materials*, vol. 271, pp. 311–320, 2014.

[10] C. S. Umpierres, P. S. Thue, E. C. Lima et al., "Microwave-activated carbons from tucumã (*Astrocaryum aculeatum*) seed for efficient removal of 2-nitrophenol from aqueous solutions," *Environmental Technology*, vol. 39, no. 9, pp. 1173–1187, 2018.

[11] J. Yener, T. Kopac, G. Dogu, and T. Dogu, "Dynamic analysis of sorption of Methylene Blue dye on granular and powdered activated carbon," *Chemical Engineering Journal*, vol. 144, no. 3, pp. 400–406, 2008.

[12] C. S. Ngakou, H. M. Ngomo, and S. G. Anagho, "Batch equilibrium and effects of ionic strength on kinetic study of adsorption of phenacetin from aqueous solution using activated carbon derived from a mixture of ayous sawdust and Cucurbitaceae peelings," *Current JournalCurrent Journal of Applied Science and TechnologyApplied Science and Technology*, vol. 26, no. 2, pp. 1–24, 2018.

[13] D. R. T. Tchuifon, S. G. Anagho, G. N. Nche, and J. M. Ketcha, "Adsorption of salicylic and sulfosalicylic acid onto powdered activated carbon prepared from rice and coffee husks," *International Journal of Current Engineering and Technology*, vol. 5, pp. 1641–1652, 2015.

[14] B. Aurelien, R. T. T. Donald, G. N. A. Nche, D. Giscard, and S. G. Anagho, "Non-linear equilibrium and kinetic study of the adsorption of 2, 4-dinitrophenol from aqueous solution using activated carbon derived from a olives stones and cotton cake," *African Journal of Environmental Science and Technology*, vol. 13, no. 9, pp. 365–380, 2019.

[15] L. A. Amola, T. Kamgaing, R. F. Tiegam Tagne, C. D. Atemkeng, I.-H. T. Kuete, and S. G. Anagho, "Optimized removal of hydroquinone and resorcinol by activated carbon based on shea residue (Vitellaria paradoxa): thermodynamics, adsorption mechanism, nonlinear kinetics, and isotherms," *Journal of Chemistry*, vol. 2022, Article ID 1125877, 15 pages, 2022.

[16] T. Kopac, "Hydrogen storage characteristics of bio-based porous carbons of different origin: a comparative review," *International Journal of Energy Research*, vol. 45, no. 15, pp. 20497–20523, 2021.

[17] K. T. Idris-Hermann, T. T. D. Raoul, D. Giscard, and A. S. Gabche, "Preparation and characterization of activated carbons from bitter kola (Garcinia kola) nut shells by chemical activation method using H_3PO_4; KOH and $ZnCl_2$," *Chemical Science International Journal*, vol. 23, no. 4, pp. 1–15, 2018.

[18] M. C. D. Ngaha, L. G. Djemmoe, E. Njanja, and I. T. Kenfack, "Biosorption isotherms and kinetics studies for the removal of 2, 6-dichlorophenolindophenol using Palm tree trunk (Elaeis guineensis)," *Journal of Encapsulation and Adsorption Sciences*, vol. 08, no. 03, pp. 156–177, 2018.

[19] M. C. D. Ngaha, E. Njanja, G. Doungmo, A. Tamo Kamdem, and I. K. Tonle, "Indigo carmine and 2, 6-dichlorophenolindophenol removal using Cetyltrimethylammonium bromide-modified Palm Oil fiber: adsorption isotherms and mass transfer kinetics," *International Journal of Biomaterials*, vol. 2019, Article ID 6862825, 18 pages, 2019.

[20] M. Hadi, M. R. Samarghandi, G. McKay, and G. McKay, "Equilibrium two-parameter isotherms of acid dyes sorption by activated carbons: study of residual errors," *Chemical Engineering Journal*, vol. 160, no. 2, pp. 408–416, 2010.

[21] G. Agbor Tabi, L. Ngouateu Rene Blaise, K. Daouda et al., "Non-linear modelling of the adsorption of Indigo Carmine dye from wastewater onto characterized activated carbon/volcanic ash composite," *Arabian Journal of Chemistry*, vol. 15, pp. 103515–103612, 2022.

[22] T. B. Gupta and D. H. Lataye, "Adsorption of indigo carmine dye onto acacia nilotica (babool) sawdust activated carbon," *Journal of Hazardous, Toxic, and Radioactive Waste*, vol. 21, no. 4, pp. 1–11, 2017.

[23] T. Oymak and E. Bagda, "Crosslinked egg white as eco-friendly, reusable and cost-effective biosorbent for rapid removal of indigo carmine," *Clean: Soil, Air, Water*, vol. 46, no. 6, Article ID 1700186, 2018.

[24] Z. Zhao, Y. Yang, L. Xu et al., "Amino acid-doped polyaniline nanotubes as efficient adsorbent for wastewater treatment," *Journal of Chemistry*, vol. 2022, Article ID 2041512, 12 pages, 2022.

[25] I.-H. T. Kuete, D. R. T. Tchuifon, G. N. Ndifor-Angwafor, A. T. Kamdem, and S. G. Anagho, "Kinetic, isotherm and thermodynamic studies of the adsorption of thymol blue onto powdered activated carbons from garcinia cola nut shells impregnated with H_3PO_4 and KOH: non-Linear regression analysis," *Journal of Encapsulation and Adsorption Sciences*, vol. 10, no. 01, pp. 1–27, 2020.

[26] P. Saha, S. Chowdhury, S. Gupta, and I. Kumar, "Insight into adsorption equilibrium, kinetics and thermodynamics of Malachite Green onto clayey soil of Indian origin," *Chemical Engineering Journal*, vol. 165, no. 3, pp. 874–882, 2010.

[27] K. Shahul Hameed, P. Muthirulan, and M. Meenakshi Sundaram, "Adsorption of Chromotrope dye onto activated carbons obtained from the seeds of various plants: equilibrium and kinetics studies," *Arabian Journal of Chemistry*, vol. 10, pp. S2225–S2233, 2017.

[28] S. Chowdhury and P. Saha, "Sea shell powder as a new adsorbent to remove basic green 4 (malachite green) from aqueous solutions: equilibrium, kinetic and thermodynamic studies," *Chemical Engineering Journal*, vol. 164, no. 1, pp. 168–177, 2010.

[29] G. Alberghina, R. Bianchini, M. Fichera, and S. Fisichella, "Dimerization of Cibacron Blue F3GA and other dyes: influence of salts and temperature," *Dyes and Pigments*, vol. 46, no. 3, pp. 129–137, 2000.

[30] S. G. Anagho, J. M. Ketcha, D. R. T. Tchuifon, and J. N. Ndi, "Kinetic and equilibrium studies of the adsorption of mercury (II) ions from aqueous solution using kaolinite and meta-kaolinite clays from Southern Cameroon," *International Journal of Research in Chemistry and Environment*, vol. 3, pp. 1–11, 2013.

[31] Y. S. Ho and G. McKay, "Pseudo-second order model for sorption processes," *Process Biochemistry (Oxford, United Kingdom)*, vol. 34, no. 5, pp. 451–465, 1999.

[32] A. A. Inyinbor, F. A. Adekola, and G. A. Olatunji, "Kinetics, isotherms and thermodynamic modeling of liquid phase adsorption of Rhodamine B dye onto Raphia hookerie fruit epicarp," *Water Resources and Industry*, vol. 15, pp. 14–27, 2016.

[33] H. N. Tran, S.-J. You, and H.-P. Chao, "Fast and efficient adsorption of methylene green 5 on activated carbon prepared from new chemical activation method," *Journal of Environmental Management*, vol. 188, pp. 322–336, 2017d.

[34] A. Gundogdu, C. Duran, H. B. Senturk et al., "Adsorption of phenol from aqueous solution on a low-cost activated carbon produced from tea industry waste: equilibrium, kinetic, and thermodynamic study," *Journal of Chemical & Engineering Data*, vol. 57, no. 10, pp. 2733–2743, 2012.

[35] N. Sharma and B. K. Nandi, "Utilization of sugarcane bagasse, an agricultural waste to remove malachite green dye from aqueous solutions," *Journal of Materials and Environmental Science*, vol. 4, no. 6, pp. 1052–1065, 2013.

[36] I. Langmuir, "The constitution and fundamental properties of solids and liquids. Part I. Solids," *Journal of the American Chemical Society*, vol. 38, no. 11, pp. 2221–2295, 1916.

[37] H. M. F. Freundlich, "Over the adsorption in solution," *Journal of Physical Chemistry*, vol. 57, pp. 385–471, 1906.

[38] M. I. Tempkin and V. Pyzhev, "Kinetics of ammonia synthesis on promoted iron catalyst," *Acta Physicochimica U.R.S.S.*vol. 12, pp. 327–356, 1940.

[39] S. Rangabhashiyam, N. Anu, M. S. Giri Nandagopal, and N. Selvaraju, "Relevance of isotherm models in biosorption of pollutants by agricultural byproducts," *Journal of Environmental Chemical Engineering*, vol. 2, no. 1, pp. 398–414, 2014.

[40] A. M. Aljeboree, A. N. Alshirifi, and A. F. Alkaim, "Kinetics and equilibrium study for the adsorption of textile dyes on coconut shell activated carbon," *Arabian Journal of Chemistry*, vol. 10, pp. 3381–3393, 2017.

[41] G. Moussavi, A. Alahabadi, and K. Yaghmaeian, "Investigating the potential of carbon activated with NH_4Cl for catalyzing the degradation and mineralization of antibiotics in ozonation process," *Chemical Engineering Research and Design*, vol. 97, pp. 91–99, 2015.

[42] A. B. Albadarin and C. Mangwandi, "Mechanisms of Alizarin Red S and Methylene blue biosorption onto olive stone byproduct: isotherm study in single and binary systems," *Journal of Environmental Management*, vol. 164, pp. 86–93, 2015.

[43] Z. Wu, H. Zhong, X. Yuan et al., "Adsorptive removal of methylene blue by rhamnolipid-functionalized graphene oxide from wastewater," *Water Research*, vol. 67, pp. 330–344, 2014.

[44] M. Saleh Bashanaini, M. H. Al-Douh, and H. S. Al-Ameri, "Removal of malachite green dye from aqueous solution by adsorption using modified and unmodified local agriculture waste," *Science Journal of Analytical Chemistry*, vol. 7, no. 2, pp. 42–56, 2019.

[45] J. K. Fatombi, E. A. Idohou, S. A. Osseni et al., "Adsorption of indigo carmine from aqueous solution by chitosan and chitosan/activated carbon composite: kinetics, isotherms and thermodynamics studies," *Fibers and Polymers*, vol. 20, no. 9, pp. 1820–1832, 2019.

[46] M. A. Ahmed, A. A. brick, and A. A. Mohamed, "An efficient adsorption of indigo carmine dye from aqueous solution on mesoporous Mg/Fe layered double hydroxide nanoparticles prepared by controlled sol-gel route," *Chemosphere*, vol. 174, pp. 280–288, 2017.

[47] A. G. S. Prado, J. D. Torres, E. A. Faria, and S. C. L. Dias, "Comparative adsorption studies of indigo carmine dye on chitin and chitosan," *Journal of Colloid and Interface ScienceColloid and Interface Science*, vol. 277, no. 1, pp. 43–47, 2004.

[48] S. M. de Oliveira Brito, H. M. C. Andrade, L. F. Soares, and R. P. de Azevedo, "Brazil nut shells as a new biosorbent to remove methylene blue and indigo carmine from aqueous solutions," *Journal of Hazardous Materials*, vol. 174, no. 1-3, pp. 84–92, 2010.

[49] R. Ahmad and R. Kumar, "Adsorptive removal of Congo red dye from aqueous solution using bael shell carbon," *Applied Surface Science*, vol. 257, no. 5, pp. 1628–1633, 2010.

[50] P. C. Bhomick, A. Supong, M. Baruah, C. Pongener, C. Gogoi, and D. Sinha, "Alizarin Red S adsorption onto biomass-based activated carbon : optimization of adsorption process parameters using Taguchi experimental design," *International journal of Environmental Science and Technology*, vol. 17, no. 2, pp. 1137–1148, 2019.

[51] C. Moreno-Castilla, "Adsorption of organic molecules from aqueous solutions on carbon materials," *Carbon*, vol. 42, no. 1, pp. 83–94, 2004.

[52] W. Wan Maznah, A. T. Al-Fawwaz, and M. Surif, "Biosorption of copper and zinc by immobilised and free algal biomass, and the effects of metal biosorption on the growth and cellular structure of chlorella sp. and chlamydomonas sp. isolated from rivers in penang, Malaysia," *Journal of Environmental Sciences*, vol. 24, no. 8, pp. 1386–1393, 2012.